RSC Advances

PAPER

View Article Online
View Journal | View Issue

Cite this: *RSC Adv.*, 2015, **5**, 54321

A simple and straightforward mechanochemical synthesis of the far-from-equilibrium zinc aluminate, $ZnAl_2O_4$, and its response to thermal treatment

Martin Fabián,*[ab] Patrick Bottke,[c] Vladimír Girman,[d] Andre Düvel,[ef] Klebson Lucenildo Da Silva,[ag] Martin Wilkening,[c] Horst Hahn,[a] Paul Heitjans[ef] and Vladimír Šepelák*[abf]

Zinc aluminate ($ZnAl_2O_4$) nanoparticles with an average size of about 10 nm are synthesized *via* one-step mechanochemical processing of the ZnO : γ-Al_2O_3 stoichiometric mixture at ambient temperature. The mechanochemically induced formation of the phase is followed by XRD and ^{27}Al MAS NMR. High-resolution TEM studies reveal a non-uniform nanostructure of mechanosynthesized aluminate consisting of ordered grains surrounded or separated by disordered surface and interfacial regions. Due to the capability of ^{27}Al MAS NMR to probe the local environment of the Al cations, valuable insights into the short-range structure of $ZnAl_2O_4$ on the Ångström length scale are provided. It is demonstrated that the as-prepared aluminate possesses a partly inverse spinel structure with a far-from equilibrium arrangement of cations and distorted polyhedra, which are spatially confined to the surface and interfacial regions with a volume fraction of *ca.* 50% and a thickness of *ca.* 1 nm. The response of the nanostructured $ZnAl_2O_4$ to subsequent thermal treatment is further investigated. It turned out that the thermally induced grain growth is accompanied by a release of microstrain, by a shrinkage of the lattice parameter, as well as by a variation in the oxygen parameter and metal–oxygen bond lengths. Evidence is given of the thermally induced redistribution of cations approaching their equilibrium positions. Upon heating above 1100 K, mechanosynthesized $ZnAl_2O_4$ relaxes towards a structural state that is similar to the bulk one.

Received 15th May 2015
Accepted 8th June 2015

DOI: 10.1039/c5ra09098a

www.rsc.org/advances

1. Introduction

The ability of spinels to redistribute their cations over crystallographically nonequivalent positions has attracted considerable interest from many scientists. The cubic spinel structure (space group $Fd\bar{3}m$) is characterized by close-packed arrays of oxygen atoms with one eighth of the tetrahedral and one half of the octahedral sites occupied by heterovalent cations (Fig. 1). To emphasize the site occupancy on the atomic level, the structural formula of 2–3 spinels of the type $M1^{2+}M2_2{}^{3+}O_4$ (where 2–3 refer to the valences of the M1 and M2 cations) may be written as $(M1_{1-\lambda}M2_{\lambda})[M1_{\lambda}M2_{2-\lambda}]O_4$, where parentheses and square brackets enclose cations that are either tetrahedrally (A) or octahedrally [B] coordinated by oxygen anions, respectively. λ represents the so-called degree of inversion that is defined as the fraction of the (A) sites occupied by trivalent (M2) cations. Spinel compounds with $\lambda = 0$ are denoted as *normal* spinels, whereas those with $\lambda = 1$ are called fully *inverse* spinels. The value of $\lambda_{rd} = 2/3$ corresponds to a random distribution of cations over the (A) and [B] positions.[1] It is well recognized that physico-chemical properties of spinels are determined to a large extent by their degree of inversion.[2–4] Thus, a detailed understanding of the functional behavior of spinels relies on careful characterization of their cation distribution.

In its equilibrium state, zinc aluminate ($ZnAl_2O_4$, gahnite) possesses the structure of a normal spinel ($\lambda_c = 0$) with the following crystal chemical formula: $(Zn)[Al_2]O_4$.[5] Considerable

[a]*Institute of Nanotechnology, Karlsruhe Institute of Technology, Hermann-von-Helmholtz-Platz 1, 76344 Eggenstein-Leopoldshafen, Germany. E-mail: fabianm@saske.sk; vladimir.sepelak@kit.edu; Fax: +49-721-60826368; Tel: +49-721-60828929*

[b]*Institute of Geotechnics, Slovak Academy of Sciences, Watsonova 45, 04001 Košice, Slovakia*

[c]*Institute for Chemistry and Technology of Materials, Graz University of Technology (NAWI Graz), Stremayrgasse 9, 8010 Graz, Austria*

[d]*Institute of Physics, Pavol Jozef Šafárik University, Park Angelinum 9, 04154 Košice, Slovakia*

[e]*Institute of Physical Chemistry and Electrochemistry, Leibniz University Hannover, Callinstr., 3-3a, 30167 Hannover, Germany*

[f]*Center for Solid State Chemistry and New Materials (ZFM), Leibniz University Hannover, Callinstr., 3-3a, 30167 Hannover, Germany*

[g]*Department of Physics, State University of Maringá, Av. Colombo 5790, 87020-900 Maringá, Brazil*

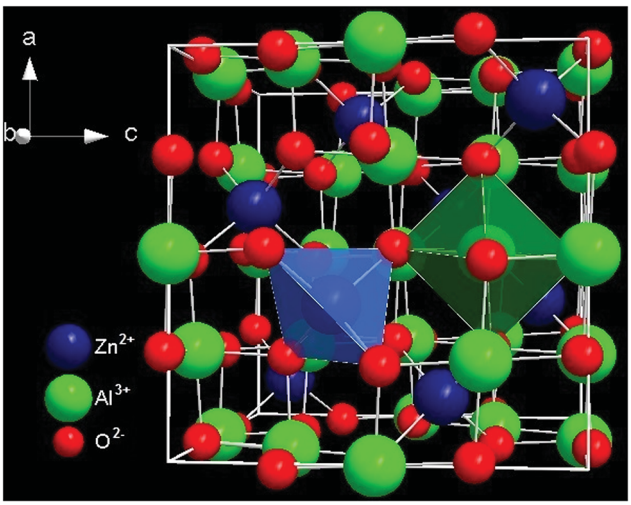

Fig. 1 Crystal structure of normal spinel $ZnAl_2O_4$ (space group *Fd*$\bar{3}$*m*). Zn^{2+} and Al^{3+} cations are distributed over the tetrahedrally (A) and octahedrally [B] coordinated sites.

attention has been paid to several of its multifunctional applications such as catalyst and catalyst support, UV-transparent support conductor, sensor, dielectric and optical material.[6–8]

The conventional solid state, *i.e.*, ceramic, synthesis of $ZnAl_2O_4$ requires long periods of calcination of the reaction precursors at considerably high temperatures.[9] In many cases, this causes the loss of zinc due to its high volatility and, consequently, it results in the formation of multiphase products and the degradation of microstructural and functional properties of the aluminate. Various wet chemistry-based routes, including, *e.g.*, hydrothermal,[10] sol–gel,[11] combustion,[12] co-precipitation,[9] complexation,[13] solvothermal[6] and sonochemical[14] methods, have also been developed to synthesize nanosized $ZnAl_2O_4$ powders. Most of the solution chemistry-based routes, however, still require calcination steps, at relatively low temperatures. Non-conventional mechanochemical synthesis (mechanosynthesis) has been recognized as an alternative low-temperature route; in general, it provides an efficient one-step and facile access to nanomaterials.[15] In this context, the present work focuses on the one-step synthesis of nanocrystalline $ZnAl_2O_4$ *via* mechanochemical processing of a ZnO + γ-Al_2O_3 mixture at ambient temperature. Although the mechanosynthesis of nanocrystalline $ZnAl_2O_4$ has already been reported in a few papers,[9,16] to the best of our knowledge there is no report in the literature focusing on the defect state or the disordered local structure of $ZnAl_2O_4$ prepared by non-conventional mechanochemical routes.

Mechanosynthesized complex oxides are often inherently unstable because of their small constituent sizes, disordered structural state, and high chemical activity.[17] To gain insight into thermal stability and relaxation of structural disorder, the present experimental work also deals with the study of the response of mechanosynthesized $ZnAl_2O_4$ when exposed to higher temperatures. For a comprehensive characterization of structural relaxation paths of the non-equilibrium product, we simultaneously apply X-ray diffraction (XRD), which is sensitive to medium- and long-range structural order, and ^{27}Al magic angle spinning (MAS) nuclear magnetic resonance (NMR), which reveals local magnetic and electronic structures. Moreover, the thermally induced evolution of the aluminate synthesized is systematically monitored with Fourier transform infrared (FTIR) spectroscopy and transmission electron microscopy (TEM).

2. Experimental

Solid precursors, zinc oxide (ZnO, 99.9% purity; Aldrich) and aluminium oxide (γ-Al_2O_3, 99% purity; Aldrich), were used for the mechanosynthesis of $ZnAl_2O_4$. 5 g of the ZnO : γ-Al_2O_3 mixture was milled for various times (up to 2 h) in a high-energy planetary ball mill (Pulverisette 7 *Premium line* (Fritsch)). A grinding chamber (80 cm^3 in volume) and balls (10 mm in diameter) made of tungsten carbide were used. The ball-to-powder weight ratio was 40 : 1. Milling experiments were performed in ambient atmosphere at 600 rpm. To investigate the thermally induced structural relaxation of mechanosynthesized $ZnAl_2O_4$, the material was subsequently annealed at various temperatures up to 1273 K in air for 4 hours.

In addition, polycrystalline $ZnAl_2O_4$ (with the average crystallite size *ca.* 105 nm) was synthesized from the mixture of ZnO and γ-Al_2O_3 precursors following a conventional ceramic process. This sample served as reference material. Note that an excess of ZnO (5 wt%) with respect to the stoichiometric ratio was used to avoid the formation of a multiphase product. In this case, powdered reactants were hand-milled, pressed into pellets and sintered at 1273 K for 24 hours. This process was repeated four times, reaching the final time of sintering of 120 hours.

The XRD patterns were collected using a D8 Advance diffractometer (Bruker) operating with Cu Kα radiation in Bragg–Brentano configuration. The generator was set up at 40 kV and 40 mA. The divergence and receiving slits were 0.3° and 0.1 mm, respectively. The patterns were recorded in the range of 20° to 105° 2θ with a step of 0.02° and a measuring time of 20 s. The JCPDS PDF database[18] was utilized for phase identification. Rietveld refinements of XRD data of the as-prepared and subsequently annealed samples were performed using the *Fullprof* computer program[19] utilizing regular Thompson–Cox–Hastings pseudo-Voigt profile parameters. In order to obtain proper geometry set-up and to eliminate instrumental broadening the instrumental resolution function was determined by the refinement of the LaB_6 standard specimen. The cubic spinel structure of $ZnAl_2O_4$ was visualized using the Diamond program.[20]

The morphology of powders was studied using a combined field-emission (scanning) transmission electron microscope (S)TEM (JEOL JEM-2100F). Prior to the TEM investigations, the powders were crushed in a mortar, dispersed in ethanol, and fixed on a copper-supported carbon grid.

^{27}Al MAS NMR measurements were performed using an Avance III 500 MHz spectrometer (Bruker) connected to an 11.4 T magnet corresponding to a Larmor frequency of 130.29 MHz for ^{27}Al. Some of the samples were measured with an Avance III 600 MHz spectrometer (14.1 T, 156.4 MHz Larmor

frequency for ^{27}Al). At both spectrometers the samples investigated were rotated in a 2.5 mm rotor at a spinning speed of 30 kHz. Typically, 64 scans were acquired with a repetition delay of 5 s. Spectra have been referenced to aqueous Al(NO_3). Since ^{27}Al is a half-integer quadrupole nucleus (spin-quantum number $I = 5/2$) we used short excitation pulses close to a $\pi/12$ pulse to record spectra being useful for a quantitative analysis of site occupancies. This is especially important for Al sites with large quadrupole coupling constants. In general, a $\pi/[4(I + 1/2)]$ pulse should be applied for such purpose.[21] Here, the degree of inversion was estimated from the intensity ratio of the NMR lines corresponding to (A)- and [B]-site Al ions, according to the formula $\lambda = 2I_{(A)}/(I_{(A)} + I_{[B]})$.

FTIR experiments were carried out using a Tensor 27 (Bruker) spectrometer. The spectra were taken in transmission mode within the range of 1200–380 cm^{-1}.

3. Results and discussion

The mechanically induced formation of $ZnAl_2O_4$ from the ZnO : γ-Al_2O_3 mixture was followed by XRD (Fig. 2). After 2 hours of intensive milling, all diffraction peaks above the background are attributed to mechanosynthesized $ZnAl_2O_4$ (JCPDS PDF 82-1043).[18] The broad shape of XRD reflections for mechanosynthesized aluminate, in contrast to the relatively narrow reflections for bulk $ZnAl_2O_4$ (see Fig. 2 at the bottom), provides clear evidence for a nanoscale nature of the oxide prepared *via* mechanosynthesis.

A representative TEM micrograph of nanocrystalline mechanosynthesized $ZnAl_2O_4$ is shown in Fig. 3. It reveals that the aluminate consists of nanoparticles with a size distribution ranging from about 5 to 40 nm; the average crystallite size (D) is estimated to be approximately 10 nm. As shown in Fig. 3a and b, the nm-sized crystallites tend to agglomerate. They are found to be roughly spherical with a so-called core–shell structure consisting of ordered inner cores (grains) surrounded or separated by disordered surface regions (see Fig. 3c). The thickness t of the disordered surface shell estimated *via* high-resolution TEM was found to be about 1 nm.

To determine the phase evolution of the ZnO : γ-Al_2O_3 mixture during high-energy milling in greater detail and to provide insight into the local structural disorder of the aluminate nanoparticles, the mechanochemical reaction was also followed by ^{27}Al MAS NMR. High-resolution NMR has been proven to be highly useful to shed light on local magnetic and electric structures around the aluminium ions. In particular, this includes also local coordination and any distortions of the oxygen polyhedra.[15,23] Fig. 4 compares ^{27}Al MAS NMR spectra of the as-prepared nanomaterial with that of the bulk $ZnAl_2O_4$ standard. The NMR spectrum of the bulk aluminate is dominated by a single line showing up at *ca.* 15 ppm which corresponds to Al ions in octahedral coordination of oxygen ions.[24] This gives evidence for a normal spinel structure ($\lambda = 0$) of the aluminate, $(Zn)[Al_2]O_4$. Note that due to the interaction of the ^{27}Al quadrupole moment with a non-vanishing electric field gradient at the Al^{3+}[B] site, which arises from an asymmetric charge distribution, the central line is perturbed by second-order quadrupole effects.[5] Such effects cannot be eliminated by magic angle spinning. The interaction manifests itself in an NMR intensity with two maxima.

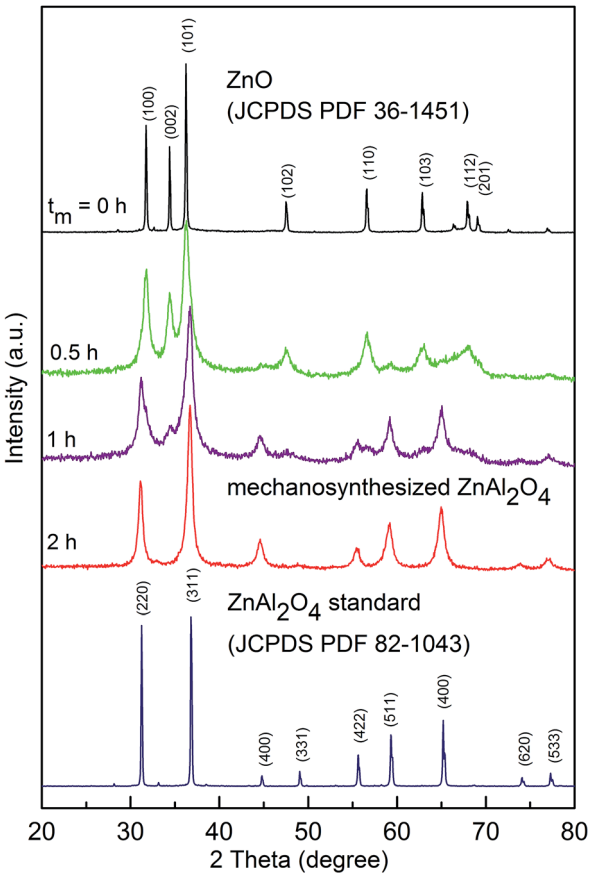

Fig. 2 XRD patterns of the ZnO : γ-Al_2O_3 mixture milled for various times (up to 2 h); the milling times, t_m, are shown in the figure. For comparison, bulk $ZnAl_2O_4$ prepared by a conventional ceramic route is shown at the bottom. Diffraction peaks of the ZnO precursor and bulk $ZnAl_2O_4$ are denoted by Miller indices. Note that any diffraction peaks of highly porous γ-Al_2O_3 are not visible due to its amorphous nature.[22]

In contrast to our reference sample, the NMR spectrum of the mechanosynthesized sample consists of two well resolved and separated lines being characteristic of tetrahedrally coordinated aluminium, Al^{3+}(A), (70 ppm) and octahedrally coordinated aluminium, Al^{3+}[B] (18 ppm). From the intensity ratio of the (A) and [B] spectral components one can estimate the cation distribution in the material; the degree of inversion of mechanosynthesized $ZnAl_2O_4$ is found to be $\lambda = 0.31(2)$. The non-equilibrium cation distribution in the nanomaterial can be characterized as follows: $(Zn_{0.7}Al_{0.3})[Zn_{0.3}Al_{1.7}]O_4$.

The change in cationic order in spinels is usually induced by high temperature,[25] high pressure,[26] irradiation of the material with electrons, ions or neutrons,[27,28] and its particle size reduction to the nanometer range.[5] All of these processing parameters were found to affect the cation distribution towards random arrangement ($\lambda \rightarrow \lambda_{rd}$).[15] For example, O'Neill and Dollase performed a detailed temperature-dependent structural study of $ZnAl_2O_4$.[29] For samples rapidly quenched from a high

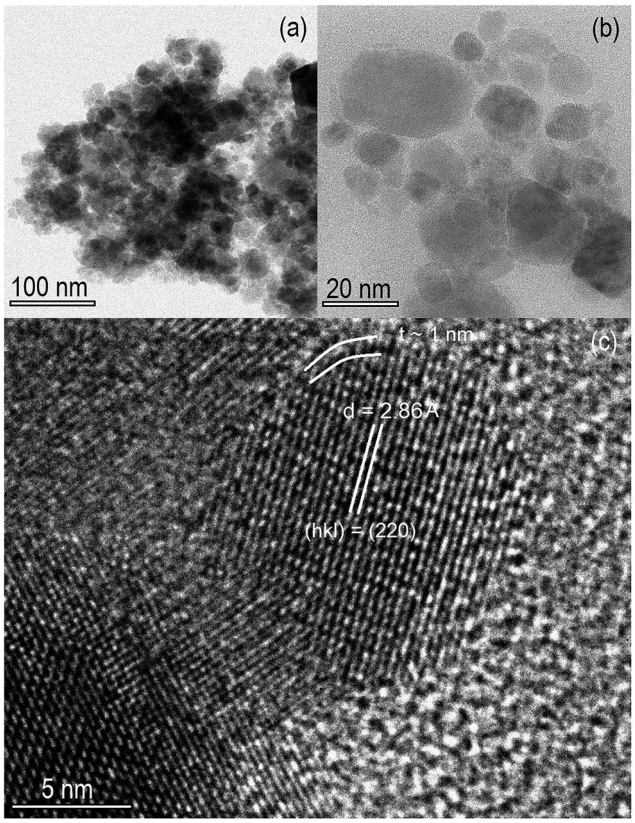

Fig. 3 (a and b) Bright-field TEM images of nanocrystalline mechanosynthesized $ZnAl_2O_4$, (c) the core–shell configuration of mechanosynthesized nanoparticles; the thickness of the surface shell ~1 nm is evident. The lattice fringes correspond to the crystallographic plane (220) (d = 2.86 Å) of the $ZnAl_2O_4$ phase (JCPDS PDF 82-1043).

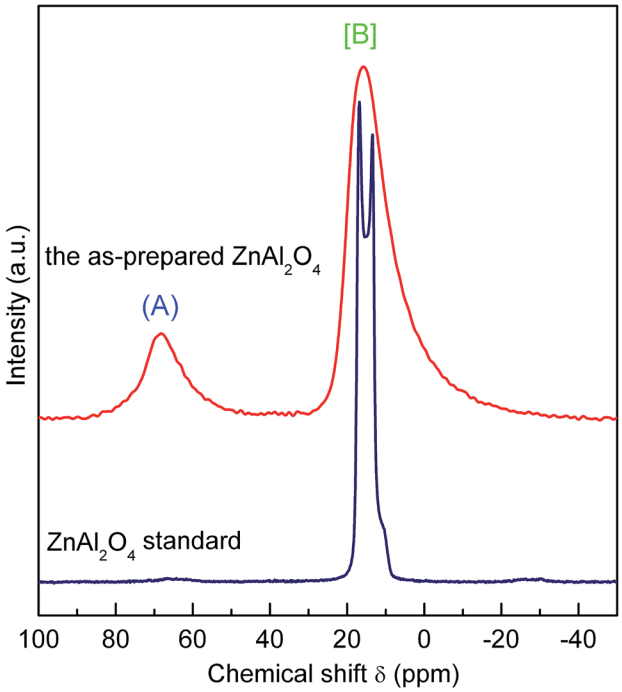

Fig. 4 Comparison of ^{27}Al MAS NMR spectra of the mechanosynthesized and the reference $ZnAl_2O_4$ recorded at 14.1 T and spinning speed of 30 kHz. The spectral peaks corresponding to (A)- and [B]-site Al ions are indicated in the figure.

temperature in the range of 973–1673 K, they found, with temperature increasing, a small increase in the degree of inversion. λ increased from 0.01 to 0.06. The extraordinary high value of $\lambda = 0.31(2)$, derived for our mechanosynthesized material, demonstrates the far-from-equilibrium nature that is accessible *via* the mechanochemical preparation route used.

By analogy with the non-uniform configuration of the mechanochemically prepared nanooxides,[15] the λ value determined for mechanosynthesized $ZnAl_2O_4$ can be considered as a mean value reflecting the cation distribution within its ordered grains and disordered interfaces and surfaces. Note that the atomic configurations in these regions of spinel oxides prepared by mechanochemical routes are chiefly characterized by a *random* arrangement of cations (λ_{rd}).[30] In contrast, the ordered grains of nano-oxides were found to exhibit an equilibrium cation distribution (λ_c).[30] Thus, the experimentally determined λ value for mechanosynthesized $ZnAl_2O_4$ can be expressed as $\lambda = (1 - w)\lambda_c + w\lambda_{rd}$, where w is the volume fraction of disordered regions. The estimated value of $w = 0.465$ indicates that about 50% of the atoms in the aluminate mechanosynthesized are in a structurally disordered state. Note that the simultaneous presence of two spinel phases characterized by different inversion parameters (λ_c and λ_{rd}) with $w = 0.80$ has also been observed in $ZnAl_2O_4$ irradiated with Au ions.[28]

Assuming a spherical shape of the as-prepared nanoparticles and taking their average diameter (D = 10 nm) as determined experimentally by TEM into account (see Fig. 3), one can deduce information on the thickness of the disordered interfacial regions in the nanomaterial [$w = 1 - (1 - 2t/D)^3$]. The resulting t, which is 0.94 nm, is comparable to the unit cell dimension (a) of the material. We note that, in general, 1 nm is a typical thickness of grain boundaries or surface shell regions in nanostructured mechanochemically prepared oxides, such as spinels, olivines, perovskites, as well as orthorhombic and ilmenite-type complex oxides.[15]

In the following, we will present and discuss the results obtained when mechanosynthesized $ZnAl_2O_4$ is exposed to higher temperatures. As it is shown in Fig. 5, subsequent annealing of $ZnAl_2O_4$ results in significant narrowing of the diffraction peaks, indicating recrystallization of the sample accompanied by crystallite growth and a release of accumulated microstrain. At temperatures above 1148 K, tiny reflections belonging to ZnO appear in the XRD pattern of the material heat treated. This is due to the thermally induced partial decomposition of the highly non-equilibrium $ZnAl_2O_4$. A similar behaviour has already been observed during thermal relaxation of mechanochemically treated $ZnFe_2O_4$.[31]

Rietveld analyses of the XRD data of the samples thermally treated enabled us to quantitatively characterize their thermally induced evolution. As is seen in Fig. 6a, the lattice parameter of the mechanosynthesized material (a = 8.121 Å) was found to be larger than that of polycrystalline $ZnAl_2O_4$ (a = 8.088 Å), which served as a reference here. The disappearance observed for the

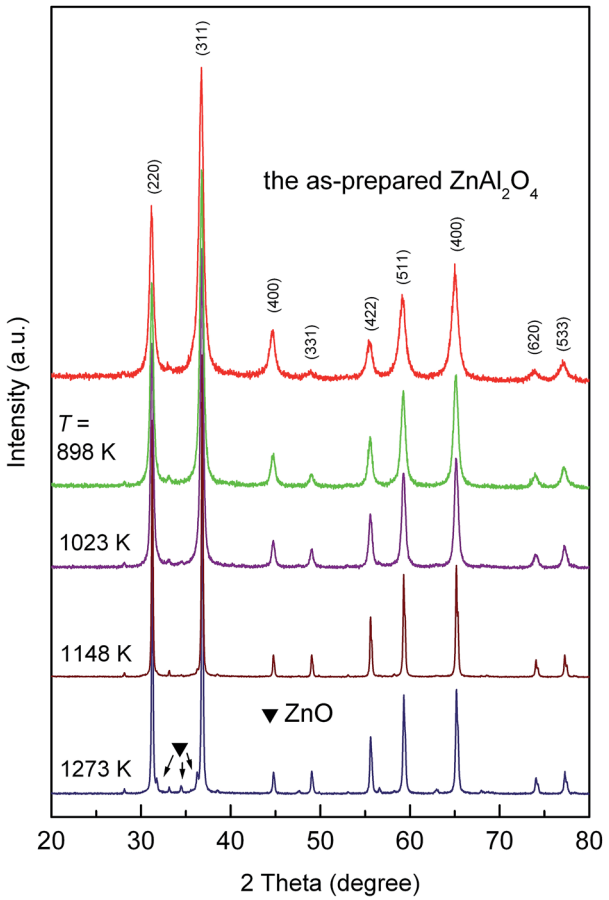

Fig. 5 XRD patterns of the as-prepared $ZnAl_2O_4$ taken after the material has been annealed for 4 hours at the temperatures indicated.

lattice expansion with increasing annealing temperature can be ascribed to a structural relaxation of the sample towards its equilibrium structure. It was found that both the crystallite size and microstrain do not change significantly with annealing temperature up to about 900 K (see Fig. 6b and c). The two properties, however, alter considerably at temperatures ranging from 900 K to 1273 K. Annealing also leads to a recovery of the local structure of the aluminate; Fig. 6d shows that the degree of inversion decreases with annealing temperature; λ changes from 0.34(2) to about 0.02(2) after treatment at 1273 K. The relaxation of the cation distribution towards its equilibrium state is accompanied by changes in the geometry of the structural units of the material. Fig. 6e shows the thermally induced variations in the cation–oxygen bond lengths in tetrahedrally and octahedrally coordinated polyhedra of $ZnAl_2O_4$. One can observe the opposite effect on the geometry of the polyhedra; while the cation–oxygen bond length in the tetrahedra expands with annealing temperature, the cation–oxygen bond length in the octahedra decreases. This alteration is obvious if we take into account the different radii of Zn^{2+} and Al^{3+} ions in (A) and [B] sites; the ions migrate from their nonequilibrium sites into the equilibrium ones; $r(Zn^{2+}) = 0.60$ Å, $r[Zn^{2+}] = 0.74$ Å, $r(Al^{3+}) = 0.39$ Å, $r[Al^{3+}] = 0.54$ Å.[32] Finally, the oxygen parameter u was found to increase with increasing annealing temperature as it is shown in Fig. 6f. For the structurally relaxed material, obtained after thermal treatment at 1273 K, this parameter takes a value of 0.264, which is close to that reported for well crystalline $ZnAl_2O_4$.[33]

The response of the mechanosynthesized aluminate to changes in temperature was also followed by ^{27}Al MAS NMR. Fig. 7 shows the ^{27}Al MAS NMR spectra of the mechanosynthesized oxide that were recorded after heat treatment at the various temperatures indicated. Annealing the sample at

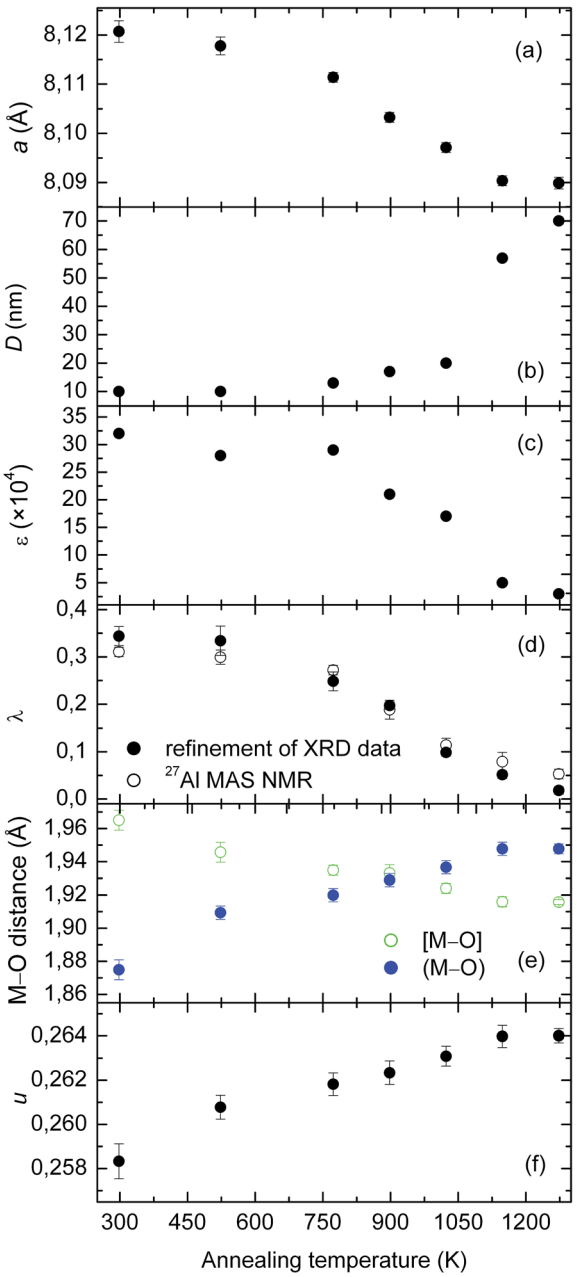

Fig. 6 Structural relaxation of the as-prepared $ZnAl_2O_4$ as a function of the annealing temperature. (a) Lattice parameter, (b) average crystallite size, (c) microstrain, (d) degree of inversion (e) cation–oxygen bond lengths for tetrahedrally (green) and octahedrally (blue) coordinated polyhedra, and (f) oxygen parameter *vs.* the annealing temperature of the mechanosynthesized $ZnAl_2O_4$.

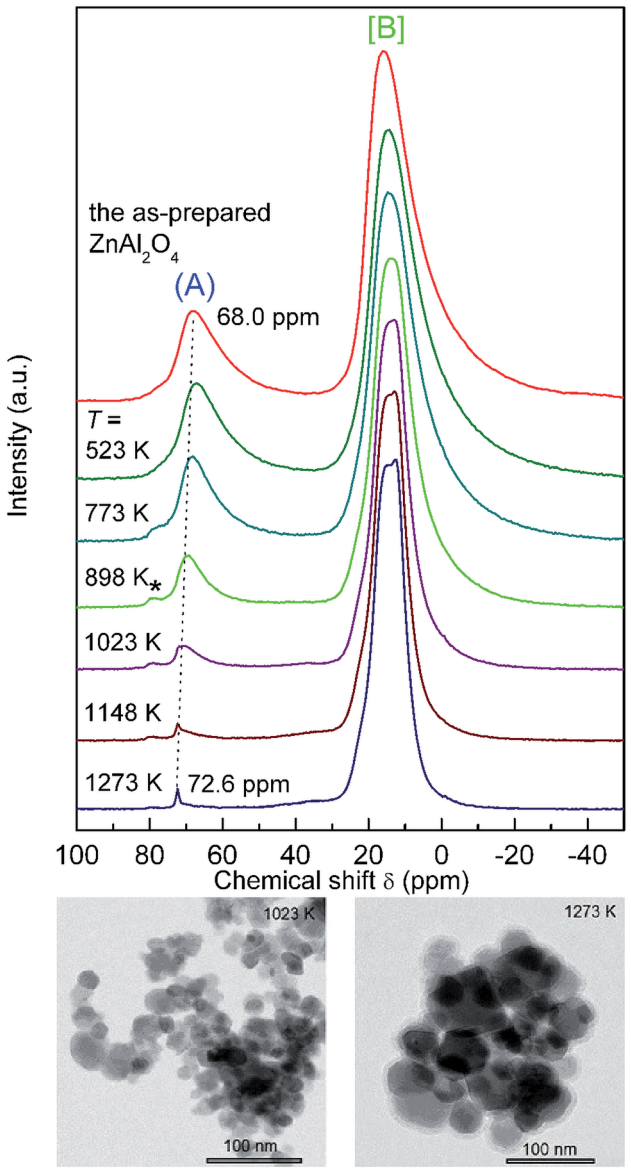

Fig. 7 (Top) ^{27}Al MAS NMR spectra of mechanosynthesized, as prepared $ZnAl_2O_4$ and of $ZnAl_2O_4$ samples that have been annealed at the temperatures indicated; the spectra were recorded at 11.4 *T*. The spectral peaks corresponding to (A)- and [B]-site Al ions are indicated. A noticeable change of chemical shifts reflects variations in the local environment of the Al nuclei; the short-dot line serves as a guide to eye. The tiny peak marked with * reveals an additional tetrahedrally coordinated Al position. (Bottom) the thermally induced growth of crystals is evident from TEM micrographs taken after treatment at 1023 K (left) and 1273 K (right).

temperatures of up to 523 K has no significant effect on the shape of the two NMR lines observed demonstrating a rather high stability of the product against heat treatment. At temperatures above 773 K, however, gradual crystallization of the $ZnAl_2O_4$ powders takes place. As expected, the spectral component corresponding to the Al^{3+}(A) ions progressively vanishes because the mechanically induced inversion of the spinel structure gets lost. This is accompanied by a gradual narrowing of the NMR line shapes implying that the octahedra

Table 1 Average crystallite size and volume fraction of interfacial regions as determined by XRD and estimated from ^{27}Al MAS NMR for mechanosynthesized $ZnAl_2O_4$ annealed at various temperatures (*T*)

T (K)	*D* (nm)	w_{XRD}	w_{NMR}
298	10	0.516	0.465
523	10	0.501	0.449
773	13	0.373	0.408
898	17	0.296	0.283
1023	20	0.148	0.171
1148	57	0.077	0.119
1273	70	0.027	0.080

are increasingly less distorted after the sample has been annealed at elevated *T*. The shift observed for the NMR lines also suggests the formation of an ordered state that is reached after heat treatment.

It is interesting to note that, most likely, the relaxation path involves an intermediate state with Al^{3+} ions located on the tetrahedral interstices 8b (see the asterisk in Fig. 7); these sites are normally not occupied by Al cations.[34] Simultaneously, with increasing temperature of heat treatment, a right-hand side broadening of the profile for the Al^{3+}[B] line (*ca.* 0 ppm) disappears. This broadening can be attributed to Al cations located in additional, most likely 16c octahedrally coordinated sites.[34,35]

The degree of inversion λ, calculated from the spectral intensities of the sample annealed at 1273 K, is approximately 0.03(3), which is well comparable with that of the reference

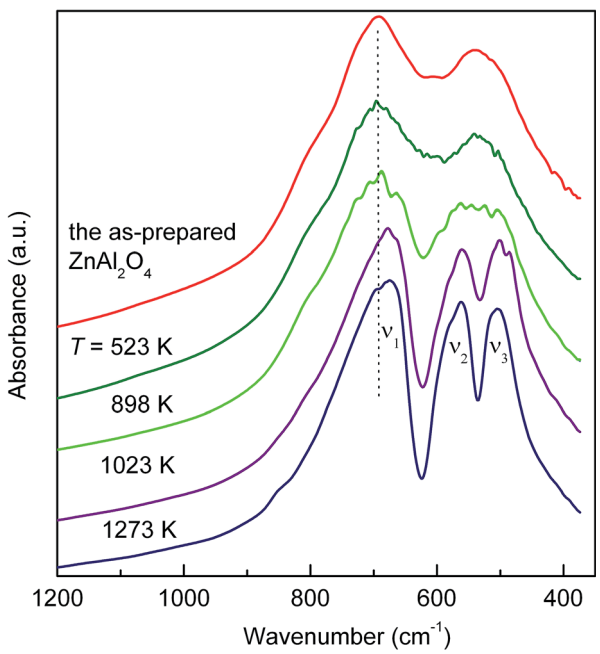

Fig. 8 FTIR spectra of the as-prepared and annealed $ZnAl_2O_4$. The shift of the absorption bands to lower wavenumbers is ascribed to the variation in the bonding force between the trivalent cation and the oxygen anion. The shoulder observed at *ca.* 790 cm^{-1} can be related to the tetrahedrally coordinated Al^{3+}.

material ($\lambda = 0.01(3)$). In detail, the results on the relaxation process of far-from-equilibrium $ZnAl_2O_4$ are listed in Table 1.

Furthermore, FTIR spectroscopy was employed to provide information on the relaxation process. As shown in Fig. 8, the spectrum of the as-prepared aluminate is dominated by two broadened bands centred at about 695 and 537 cm^{-1}. They can be assigned to stretching vibrations in the oxide. A shoulder at about 790 cm^{-1} can be related to the vibrations of Al^{3+}(A) ions.[36,37] With increasing annealing temperature the absorption bands become sharper and the peak centred at 537 cm^{-1} splits into two absorption maxima at $\nu_2 = 564$ cm^{-1} and $\nu_3 = 504$ cm^{-1}. This can be ascribed to the relaxation of the geometry of distorted polyhedra in $ZnAl_2O_4$. Since the position of vibrational modes is rather sensitive to the chemical nature of trivalent cations, *i.e.*, to the bonding force between a trivalent cation and an oxygen anion,[38] the observed red shift indicates the redistribution of cations from their nonequilibrium sites towards the equilibrium ones. The latter is accompanied by the gradual disappearance of the shoulder at 790 cm^{-1}.

4. Conclusions

The present study demonstrates that nanostructured $ZnAl_2O_4$ with an average crystallite size of about 10 nm in diameter can be prepared *via* simple and straightforward mechanochemical synthesis starting with a stoichiometric mixture of $ZnO : \gamma\text{-}Al_2O_3$. The synthesis was carried out at ambient temperature and the reaction time was relatively short (2 h). It has been found that the as-prepared, nanostructured aluminate consists of ordered crystalline grains surrounded or separated by disordered interfacial regions characterized by a volume fraction of about 50%. ^{27}Al MAS NMR spectroscopy demonstrates that the nano-aluminate is characterized by distorted polyhedra; moreover, the oxide shows a far-from equilibrium arrangement of cations characterized by degree of inversion of $\lambda = 0.31(2)$. Fortunately, the range of thermal stability of the mechanosynthesized product extends up to *ca.* 523 K. Upon annealing at $T > 773$ K, the nonequilibrium cation distribution relaxes towards the equilibrium configuration. Simultaneously, the crystallites grow and the accumulated microstrain releases during annealing. This relaxation process is accompanied by a disappearance of the lattice expansion and variations in the cation–oxygen bond lengths. Thus, during heating, mechanosynthesized $ZnAl_2O_4$ relaxes towards a structural state that is similar to that of the bulk oxide.

Acknowledgements

The support by the DFG within the framework of the Priority Program "*Crystalline Nonequilibrium Phases*" (SPP 1415, grants no.: WI 3600 5-2 and HE 1574 11-2) and the VEGA (projects 2/0097/13 and 2/0097/14) is gratefully acknowledged. M.F. thanks "*Action Austria-Slovakia*" cooperation programme for support of his work at TU Graz. V.Š. acknowledges additional support by the APVV (0528-11).

Notes and references

1 V. Šepelák, S. M. Becker, I. Bergmann, S. Indris, M. Scheuermann, A. Feldhoff, C. Kübel, M. Bruns, N. Stürzl, A. S. Ulrich, M. Ghafari, H. Hahn, C. P. Grey, K. D. Becker and P. Heitjans, *J. Mater. Chem.*, 2012, **22**, 3117.
2 V. Šepelák, I. Bergmann, D. Menzel, A. Feldhoff, P. Heitjans, F. J. Litterst and K. D. Becker, *J. Magn. Magn. Mater.*, 2007, **316**, 764.
3 J. Wu, Z. Huang, W. Zhou, C. Ouyang, Y. Hou, Y. Gao, R. Chen and J. Chu, *J. Appl. Phys.*, 2014, **115**, 113703.
4 A. Kan, T. Moriyama, S. Takhashi and H. Ogawa, *Jpn. J. Appl. Phys.*, 2013, **52**, 09KH01.
5 V. Šepelák, I. Bergmann, S. Indris, A. Feldhoff, H. Hahn, K. D. Becker, C. P. Grey and P. Heitjans, *J. Mater. Chem.*, 2011, **21**, 8332.
6 W. Staszak, M. Zawadzki and J. Okal, *J. Alloys Compd.*, 2010, **492**, 500.
7 N. J. van der Laag, M. D. Snel, P. C. M. M. Magusin and G. de With, *J. Eur. Ceram. Soc.*, 2004, **24**, 2417.
8 X. Y. Chen, C. Ma, Z. J. Zhang and B. N. Wang, *Mater. Sci. Eng., B*, 2008, **151**, 224.
9 A. D. Ballarini, S. A. Bocanegra, A. A. Castro, S. R. de Miquel and O. A. Scelza, *Catal. Lett.*, 2009, **129**, 293.
10 K. Sakoda and M. Hirano, *Ceram. Int.*, 2014, **40**, 15841; H. Zhao, Y. Dong, P. Jiang, G. Wang, J. Zhang and C. Zhang, *Chem. Eng. J.*, 2015, **260**, 623; M. Y. Guan, D. M. Xu, Y. F. Song and Y. Guo, *Sens. Actuators, B*, 2013, **188**, 1148; Z. Chen, E. Shi, W. Li, Y. Zheng, N. Wu and W. Zhong, *J. Am. Ceram. Soc.*, 2002, **85**, 2949.
11 R. K. Sharma and G. Ranjana, *Ceram. Int.*, 2014, **40**, 3209; M. S. Zulfakar, H. Abdullah, W. N. W. Jalal, S. Shaari and Z. Zainuddin, *Adv. Mater. Res.*, 2014, **895**, 63; X. Duan, D. Yuan, X. Wang and H. Xu, *J. Sol-Gel Sci. Technol.*, 2005, **35**, 221.
12 R. Ianos, S. Borcănescu and R. Lazău, *Chem. Eng. J.*, 2014, **240**, 260.
13 C. G. Anchieta, D. Sallet, E. L. Foletto, S. S. da Silva, O. Chiavone-Filho and C. A. O. do Nascimento, *Ceram. Int.*, 2014, **40**, 4173.
14 D. P. Dutta, R. Ghildiyal and A. K. Tyagi, *J. Phys. Chem. C*, 2009, **113**, 16954.
15 V. Šepelák, A. Düvel, M. Wilkening, K.-D. Becker and P. Heitjans, *Chem. Soc. Rev.*, 2013, **42**, 7507.
16 M. V. Zdujić, O. B. Milošević and L. Č. Karanović, *Mater. Lett.*, 1992, **13**, 125.
17 K. L. Da Silva, D. Menzel, A. Feldhoff, C. Kübel, M. Bruns, A. Paesano Jr, A. Düvel, M. Wilkening, M. Ghafari, H. Hahn, F. J. Litterst, P. Heitjans, K. D. Becker and V. Šepelák, *J. Phys. Chem. C*, 2011, **115**, 7209.
18 Joint Committee on Powder Diffraction, Standards (JCPDS) Powder Diffraction File (PDF), International Centre for Diffraction Data, Newtown Square, PA, 2004.
19 J. Rodriguez-Carvajal, *Fullprof Program, Version 2.4.2*, ILL Grenoble, Grenoble, France, 1993.

20 K. Brandenburg and H. Putz, *Diamond—Crystal and Molecular Structure Visualization Software, Version 3.0a*, Crystal Impact GbR, Bonn, Germany, 2004.
21 D. Fenzke, D. Freude, T. Fröhlich and J. Haase, *Chem. Phys. Lett.*, 1984, **111**, 171; D. Massiot, C. Bessada, J. P. Coutures and F. Taullele, *J. Magn. Reson.*, 1990, **90**, 231.
22 L. Samain, A. Jaworski, M. Edén, D. M. Ladd, D.-K. Seo, F. J. Garcia-Garcia and U. Häussermann, *J. Solid State Chem.*, 2014, **217**, 1.
23 A. Düvel, E. Romanova, M. Sharifi, D. Freude, M. Wark, P. Heitjans and M. Wilkening, *J. Phys. Chem. C*, 2011, **115**, 22770.
24 R. L. Millard, R. C. Peterson and B. K. Hunter, *Am. Mineral.*, 1992, **77**, 44.
25 S. A. T. Redfern, R. J. Harrison, H. S. C. O'Neill and D. R. R. Wood, *Am. Mineral.*, 1999, **84**, 299.
26 Z. Wang, P. Lazor, S. K. Saxena and G. Artioli, *J. Solid State Chem.*, 2002, **165**, 165.
27 T. Soeda, S. Matsumura, C. Kinoshita and N. J. Zaluzec, *J. Nucl. Mater.*, 2000, **283–287**, 952.
28 G. Baldinozzi, D. Simeone, D. Gosset, M. Dollé, L. Thomé and L. Mazérolles, *Nucl. Instrum. Methods Phys. Res., Sect. B*, 2006, **250**, 119.
29 H. S. C. O'Neill and W. A. Dollase, *Phys. Chem. Miner.*, 1994, **20**, 541.
30 V. Šepelák, I. Bergmann, A. Feldhoff, P. Heitjans, F. Krumeich, D. Menzel, F. J. Litterst, S. J. Campbell and K. D. Becker, *J. Phys. Chem. C*, 2007, **111**, 5026.
31 V. Šepelák, L. Wilde, U. Steinike and K. D. Becker, *Mater. Sci. Eng., A*, 2004, **375–377**, 865.
32 R. D. Shannon, *Acta Crystallogr. A*, 1976, **32**, 751.
33 M. Ardit, G. Cruciani and M. Dondi, *Am. Mineral.*, 2012, **97**, 1394.
34 K. E. Sickafus, J. M. Wills and N. W. Grimes, *J. Am. Ceram. Soc.*, 1999, **82**, 3279.
35 V. Sreeja, T. S. Smitha, D. Nand, T. G. Ajithkumar and P. A. Joy, *J. Phys. Chem. C*, 2008, **112**, 14737; H. Maekawa, S. Kato, K. Kawamura and T. Yokokawa, *Am. Mineral.*, 1997, **82**, 1125.
36 A. A. Da Silva, A. D. S. Conçalves and M. R. Davolos, *J. Sol-Gel Sci. Technol.*, 2009, **49**, 101.
37 P. Tarte, *Spectrochim. Acta*, 1967, **23**, 2127.
38 J. Preudhomnei and P. Tarte, *Spectrochim. Acta*, 1971, **27**, 1817.

